Journal of Materials Science: Materials in Electronics (2020) 31:17029–17035
https://doi.org/10.1007/s10854-020-04260-3

Influence of Li_2O–MgO–ZnO–B_2O_3–SiO_2 glass doping on the microwave dielectric properties and sintering temperature of $Li_3Mg_2NbO_6$ ceramics

Xiaohua Zhou[1] · Xiaoqing Ning[1] · Xing Zhang[1] · Dawei Xia[1] · Bin Tang[1] · Shuren Zhang[1]

Received: 22 June 2020 / Accepted: 13 August 2020 / Published online: 24 August 2020

Abstract
$Li_3Mg_2NbO_6 + x$ wt% Li_2O–MgO–ZnO–B_2O_3–SiO_2 (LMZBS, $x = 2, 4, 6, 8, 10$) microwave dielectric ceramics with the rock-salt structure were primarily investigated by the traditional solid-state method. The microstructures, microwave dielectric properties, and sintering characteristics were studied systematically according to the doping concentration and sintering temperature. It could be seen that the LMZBS glass effectively lower the sintering temperature of $Li_3Mg_2NbO_6$ ceramics from 1250 to 925 °C with microwave dielectric properties changing as a function of the amounts of the LMZBS glass. The experimental results showed that 4 wt% LMZBS glass enabled $Li_3Mg_2NbO_6$ ceramics sintered at 925 °C for 4 h to have excellent microwave dielectric properties: $\varepsilon_r = 16.02$, $Q \times f = 56{,}455$ GHz, $\tau_f = -18.81$ ppm/°C. Therefore, $Li_3Mg_2NbO_6$ ceramics doped with LMZBS glass meet the requirements of low-temperature co-fired ceramics.

1 Introduction

Microwave dielectric ceramics are one of the functional ceramic materials, which refer to the ceramic materials used in the microwave frequency band (300 MHz–300 GHz) [1, 2]. Low-temperature co-fired ceramics (LTCC) are formed by sintering ceramic matrix materials with low-resistivity metal conductors (such as silver, copper, etc.) under low-temperature conditions normally below 960 °C [3]. With the development of electronic materials technology [4–6], the requirements of electronic components in terms of performance and functions are increasing, while the compact size of products cannot be sacrificed. Therefore, the LTCC technology has been widely used in the field of microelectronics. However, the preparation of high-performance dielectric materials is generally associated with higher sintering temperatures, so exploring high-performance dielectric materials under low-temperature sintering has gained more attention. Generally speaking, three universal methods are used to allow the materials to reach the densification temperature of LTCC at temperatures below 960 °C and maintain excellent dielectric properties. The first method is based on the glass ceramics or the filled glass ceramic composites. The next is based on the low-melting point glass or compound by virtue of liquid phase. The last method is a new microwave dielectric ceramic system with inherently low sintering temperature [7]. The glass–ceramic system can be used to adjust the dielectric properties, the sintering temperature, the bending strength and the thermal expansion coefficient, etc. Therefore, the best choice to obtain low-cost and high-performance LTCC materials is to find a new suitable glass ceramic system to reduce the current ceramic sintering temperature [8].

Recently, there were many reports about improved performance of $Li_3Mg_2NbO_6$ ceramics by doping [9, 10]. In 2009, Yuan et al. [11] discovered that $Li_3Mg_2NbO_6$ can achieve excellent microwave dielectric properties at 1250 °C of $\varepsilon_r = 16.8$, $Q \times f = 79{,}643$ GHz, $\tau_f = -27.2$ ppm/°C. Therefore, $Li_3Mg_2NbO_6$ microwave dielectric ceramics have received extensive interests. Then Pan et al. [12] first reported the low sintering temperature characteristic of $Li_3Ni_2NbO_6$ in 2017, which could be sintered into porcelain at 850 °C with dielectric properties of $\varepsilon_r = 15.85$, $Q \times f = 19{,}860$ GHz, $\tau_f = -15.45$ ppm/°C. Zhang et al. [13] utilized the Li_2O–B_2O_3–SiO_2 glass doping to reveal that $Li_3Mg_2NbO_6$ − 1.0 wt% LBS ceramic has practical dielectric properties at 875 °C of $\varepsilon_r = 14.89$, $Q \times f = 86{,}720$ GHz,

✉ Xiaohua Zhou
zxh_uestc@163.com

[1] School of Electronic Science and Engineering, University of Electronic Science and Technology of China, Chengdu 610054, People's Republic of China

$\tau_f = -15.46$ ppm/°C. Wang et al. [14] used $CaCO_3$ and LMZBS glass doping to adjust both τ_f and sintering temperature and reported that the dielectric properties of $Li_3Mg_{1.8}Ca_{0.2}NbO_6$ − 1 wt% LMZBS fired at 950 °C were $\varepsilon_r = 16.70$, $Q \times f = 31{,}000$ GHz, $\tau_f = -1.3$ ppm/°C. Wang et al. [15] also used TiO_2 to adjust the frequency temperature coefficient of $Li_3Mg_2NbO_6$ to obtain a near-zero frequency temperature coefficient and reported its performance was $\varepsilon_r = 16$, $Q \times f = 42{,}648$ GHz, $\tau_f = -1$ ppm/°C.

As an effective sintering additive, the LMZBS glass performed well in Al_2O_3 and other systems simultaneously lowering temperature and preserving dielectric properties [16, 17], but its effect on $Li_3Mg_2NbO_6$ pure phase ceramics has not been reported. Therefore, it was very important to study the effect of LMZBS glass on the sintering behavior and microwave dielectric properties of $Li_3Mg_2NbO_6$ pure phase ceramics. In our work, $Li_3Mg_2NbO_6$ ceramics were prepared by the traditional solid-state method using the LMZBS glass as a sintering dopant. The effects of LMZBS glass on the sintering characteristics, microstructure and microwave dielectric properties of $Li_3Mg_2NbO_6$ ceramics were investigated and concluded.

2 Experimental

According to the stoichiometric ratio of $Li_3Mg_2NbO_6$ molecular formula, $Li_3Mg_2NbO_6$ ceramics were prepared by mixing three materials of Li_2CO_3 (99%), MgO (98.5%) and Nb_2O_5 (99%). Then the planetary grinder which at a speed of 280 rpm was used to grind the raw material with the ZrO_2 ball and deionized water for 6 h, that the mass fraction ratio was ZrO_2 ball: deionized water: raw material = 5: 1.2: 1. The mixtures were sieved with the 60-purpose sieve after drying at 110 °C. Then $Li_3Mg_2NbO_6$ powders were made after sintering the for 4 h at 1000 °C. Li_2O–MgO–ZnO–B_2O_3–SiO_2 glass was made of Li_2CO_3 (99%), MgO (98.5%), ZnO (99%), H_3BO_3 (99%), SiO_2 (99%), and its mass fraction ratio was Li_2CO_3:MgO:ZnO:H_3BO_3:SiO_2 = 10:32:8:41:9, which was prepared by conventional glass processing. Then, mixtures were ground again for 8 h with the parameter of the first water grinding after adding 2–10 wt% LMZBS glass in $Li_3Mg_2NbO_6$ powders. Acrylic acid was used as an adhesive after mixtures were dried, and the powders were pressed into a cylinder with a diameter of 15 mm and a height of about 6 mm. Finally, the mixtures were sintered in the air for 4 h at the temperatures of 875 °C to 950 °C, and the heating speed of the high-temperature furnace was 3 °C/min.

The crystal phase of the sintered sample was determined by X-ray diffraction (XRD, Philips X'Pert Pro MPD, The Nether-lands) with 45 kV and 40 mA CuKα alpha radiation. Scanning electron microscopy [SEM, FEI Inspect F, UK coupled with energy-dispersive X-ray spectroscopy (EDS)] was used to analyze the microstructure of ceramic surfaces after sintering. The bulk density values were measured by the Archimedes drainage method. The microwave dielectric characteristics were studied by the Hakki-Coleman dielectric resonator method in TE011 mode according to the vector network analyzer (HP83752A, USA). The resonance frequency data of the samples were measured at 25 °C and 85 °C, the temperature coefficient of resonant frequency was obtained by the following formula [18]:

$$\tau_f = \frac{1}{f_{25}} \times \frac{1}{60} \times (f_{85} - f_{25}) \times 10^6 (ppm/^\circ C) \quad (1)$$

where the f_{25} represents the resonance frequency of 25 °C and the f_{85} represents the resonance frequency of 85 °C.

3 Results and discussion

Figure 1 illustrates the relationship between bulk density of $Li_3Mg_2NbO_6$ composite ceramics and different doping amount of LMZBS glass as well as different sintering temperatures. The factors that affect the bulk density are the type of material, the sintering temperature and the state of the material [19]. From the change of the curve, the bulk densities firstly increase and then decrease with the increase of the sintering temperature. The bulk densities reach the highest at 925 °C, indicating the idea sintering temperature is around 925 °C for all of the specimens that were doped with various amounts of the LMZBS sintering aid. Besides, as the doping amount of LMZBS glass increases, the bulk densities rise to the highest values with the doping amount of 4 wt% LMZBS glass, and then decrease.

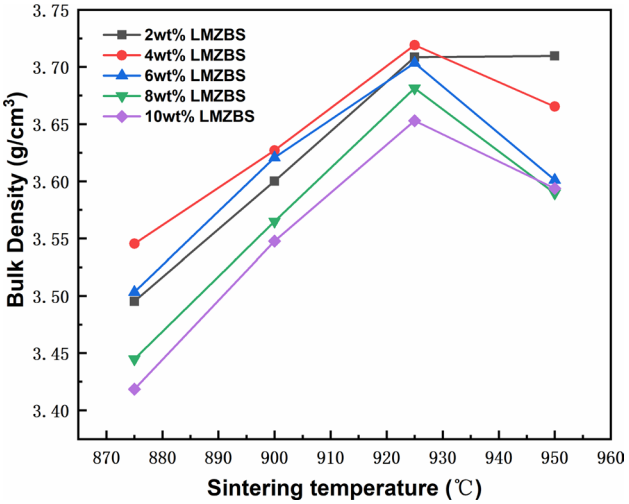

Fig. 1 The bulk density of $Li_3Mg_2NbO_6 + x$ wt% LMZBS ($x = 2$–10) ceramics sintered at 875–925 °C for 4 h

The lattice parameter, unit cell volume, theoretical density, bulk density and relative density of $Li_3Mg_2NbO_6$ at 925 °C for 4 h under different amounts of doped LMZBS glass are illustrated in Table 1. The Jade software was used to fit sample's diffraction peaks by the Rietveld refinement method. And the result of the Rietveld refinement method could get the unit cell parameters and the lattice constants of the sample. Generally, the unit cell volume will increase with the increase of the interplanar distance, so the unit cell volume increases with the increase of x. The relative density is obtained by the following formula:

$$\rho_{relative} = \frac{\rho_a}{\rho_{theo}} \times 100\% \quad (2)$$

where $\rho_{relative}$ is the relative density, ρ_a is the bulk density, and ρ_{theo} is the theoretical density.

The theoretical density should be calculated from the below equation [20]:

$$\rho_{theo} = \frac{n \times A}{V \times N} \quad (3)$$

where n is the number of atoms in unit cell, A is the atom weight, V is the volume of unit cell, and N is the Avogadro number.

It can be seen from Table 1 that the relative density reaches the maximum when doping 4 wt% content of LMZBS glass on $Li_3Mg_2NbO_6$ ceramics. The results are in line with the bulk density curve in Fig. 1.

Figure 2a presents the X-ray diffraction patterns of $Li_3Mg_2NbO_6 + x$ wt% LMZBS ($x = 2$–10) ceramics sintered at 925 °C for 4 h. It can be detected from XRD that the main crystal phase is $Li_3Mg_2NbO_6$ phase (JCPDS # 86-0346) of an orthorhombic rock-salt structure with a space group of Fddd. However, there are impure phases observed, which may be related to the addition of the LMZBS glass. The appearance of the impure phases is confirmed by the element concentration results obtained by the EDS analysis. From the results of the single peak search and the element concentration content by EDS analysis, the impure phases contain SiO_2 phase and Mg_2SiO_4 phase. The amplifying XRD diagram in Fig. 2b presents that the height of the diffraction peaks decreases and the position of the diffraction peaks shifts with the increase of the LMZBS glass content.

Table 1 The lattice parameters, unit cell volume (*V*unit), density (ρ_{theo}, ρ_a, $\rho_{relative}$) of $Li_3Mg_2NbO_6 + x$ wt% LMZBS ($x = 2$–10) ceramics sintered at 925 °C for 4 h

$Li_3Mg_2NbO_6 - x$ wt% LMZBS	Lattice parameters				ρ_{theo} (g/cm^3)	ρ_a (g/cm^3)	$\rho_{relative}$ (%)
	a (Å)	*b* (Å)	*c* (Å)	*V* (Å^3)			
$x = 2$	5.8946	8.5391	17.7188	891.879	3.8477	3.7085	96.38
$x = 4$	5.8955	8.5390	17.7205	892.076	3.8468	3.7191	96.68
$x = 6$	5.8959	8.5405	17.7220	892.368	3.8430	3.7034	96.36
$x = 8$	5.8968	8.5398	17.7222	892.438	3.8452	3.6814	95.74
$x = 10$	5.8972	8.5412	17.7249	892.793	3.8437	3.6530	95.04

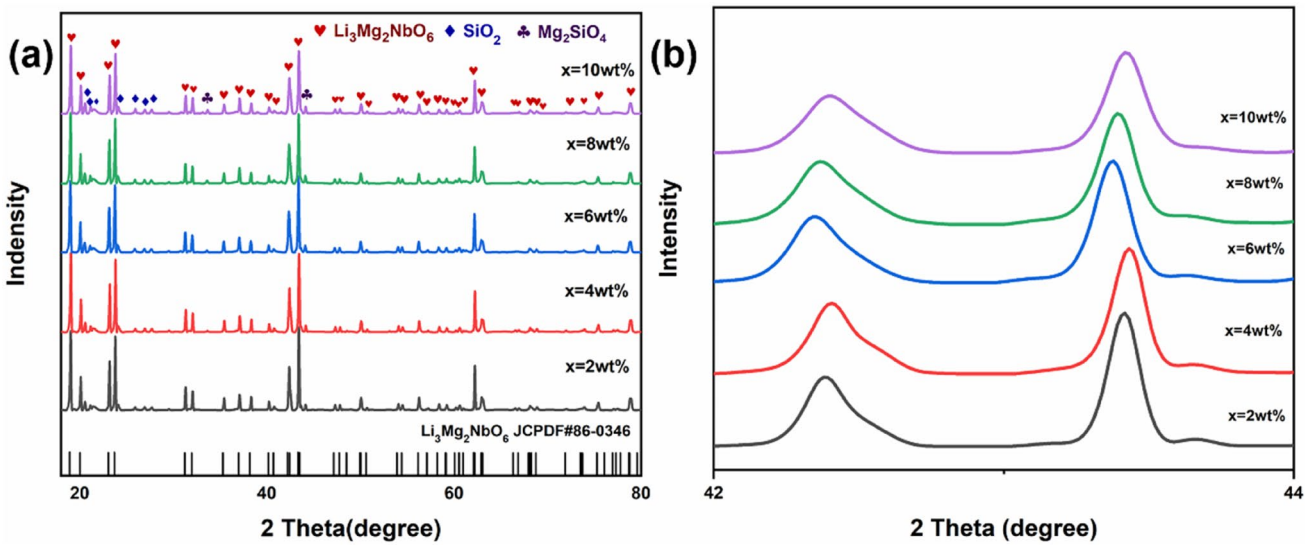

Fig. 2 The XRD patterns of the $Li_3Mg_2NbO_6 + x$ wt% LMZBS ($x = 2$–10) ceramics sintered at 925 °C for 4 h (**a**) and variation of the diffraction peak (**b**)

Figure 3 demonstrates the SEM images of the $Li_3Mg_2NbO_6 + x$ wt%LMZBS ($x = 2$–10) ceramics sintered at 925 °C for 4 h. The porosity decreased and the grain size increased with the elevated content of LMZBS glass, which indicates that the suitable LMZBS glass contributes to the densification of ceramics. It can be found from the figures that the position of the impurities is at the grain boundaries of the $Li_3Mg_2NbO_6$ phase. Besides, the amount of grains of the impure phase increases as the content of LMZBS glass increases. Therefore, it can be concluded that the LMZBS glass causes the grains of $Li_3Mg_2NbO_6$ to aggregate through the capillary force at the grain boundaries which can promote the densification of the ceramic.

Figure 4 shows the EDS analysis of $Li_3Mg_2NbO_6 + 4$ wt% LMZBS ceramics sintered at 925 °C for 4 h. It should be noted that the lithium elements cannot be detected by the EDS due to their light weight. The element concentration content at Spot A was conformed to the element concentration of $Li_3Mg_2NbO_6$ ceramics as shown in Fig. 4a. Besides, the element concentration content of the impurity in the grain boundaries at Spot B does not match the element concentration of $Li_3Mg_2NbO_6$ as shown in Fig. 4b. Obviously, there may be more LMZBS glass at Spot B. The results of the EDS analysis are in line with the observation results of the SEM pictures.

Figure 5 depicts the varying dielectric constants with doping amount of LMZBS glass as well as different sintering temperatures, which matches the variation trend of the bulk density curve. The dielectric constant often depends on the crystal structure, dielectric polarization, relative density, and other phase content [21]. Therefore, the dielectric constant is affected by the change of LMZBS glass content and sintering temperatures, together with the influence of the bulk density. Besides, the shifted crystal structure of $Li_3Mg_2NbO_6$ ceramics and the appearance of impure phases also affect the dielectric constant to a certain extent.

Figure 6 exhibits the $Q \times f$ values of the $Li_3Mg_2NbO_6 + x$ wt% LMZBS ($x = 2$–10) ceramics sintered at 875–950 °C for 4 h. The quality factor values increase when sintering at 875 to 925 °C for 4 h, then decrease when the sintering temperature increase to 950 °C. The result again proves that the ideal sintering temperature is 925 °C for the LMZBS-doped $Li_3Mg_2NbO_6$ ceramics in this study. For different doping amounts of LMZBS glass, the quality factor values reach the peaks when doping content is 4 wt% LMZBS glass. Therefore, the best quality factor value is got when

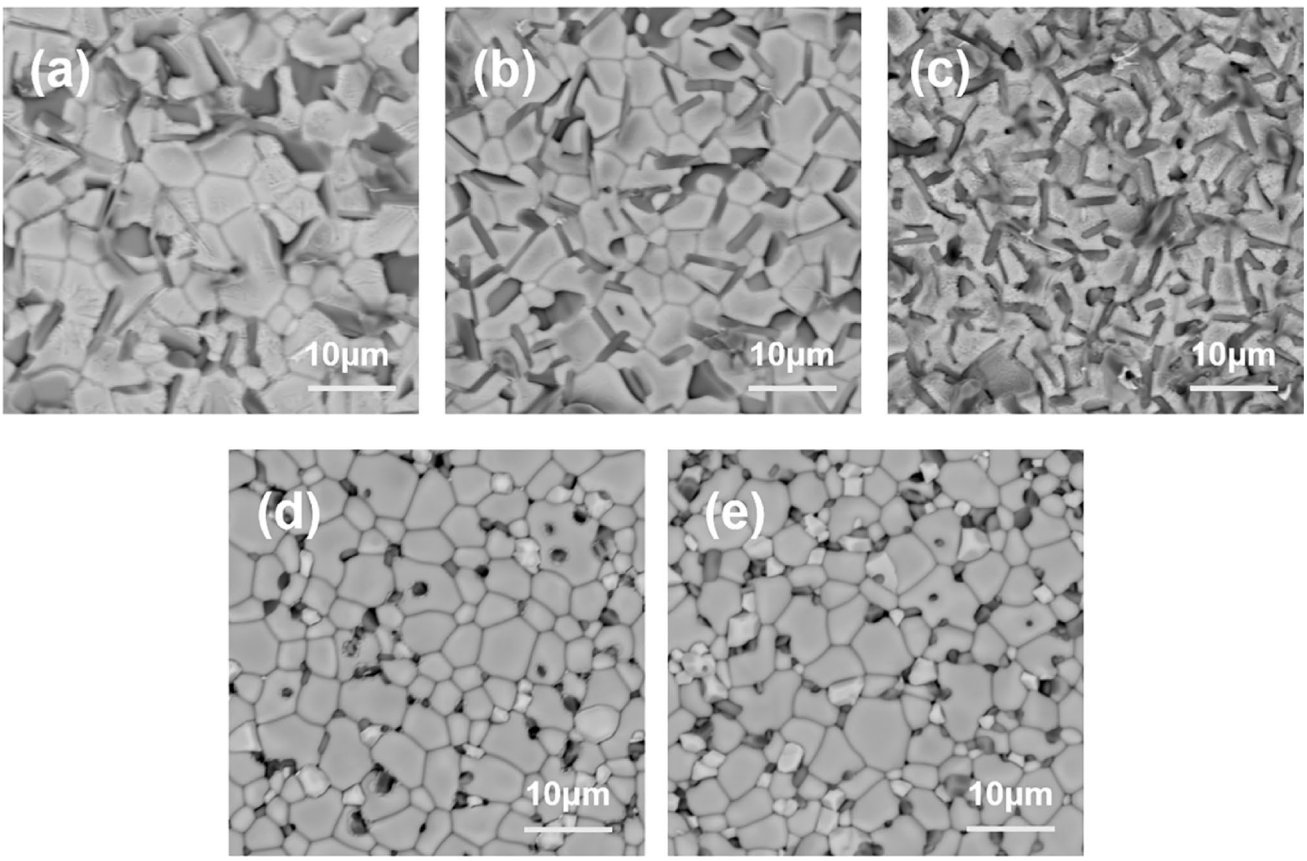

Fig. 3 The SEM photographs of the $Li_3Mg_2NbO_6$ ceramics sintered at 925 °C for 4 h, modified with **a** 2 wt%, **b** 4 wt%, **c** 6 wt%, **d** 8 wt%, and **e** 10 wt% of the LMZBS glass

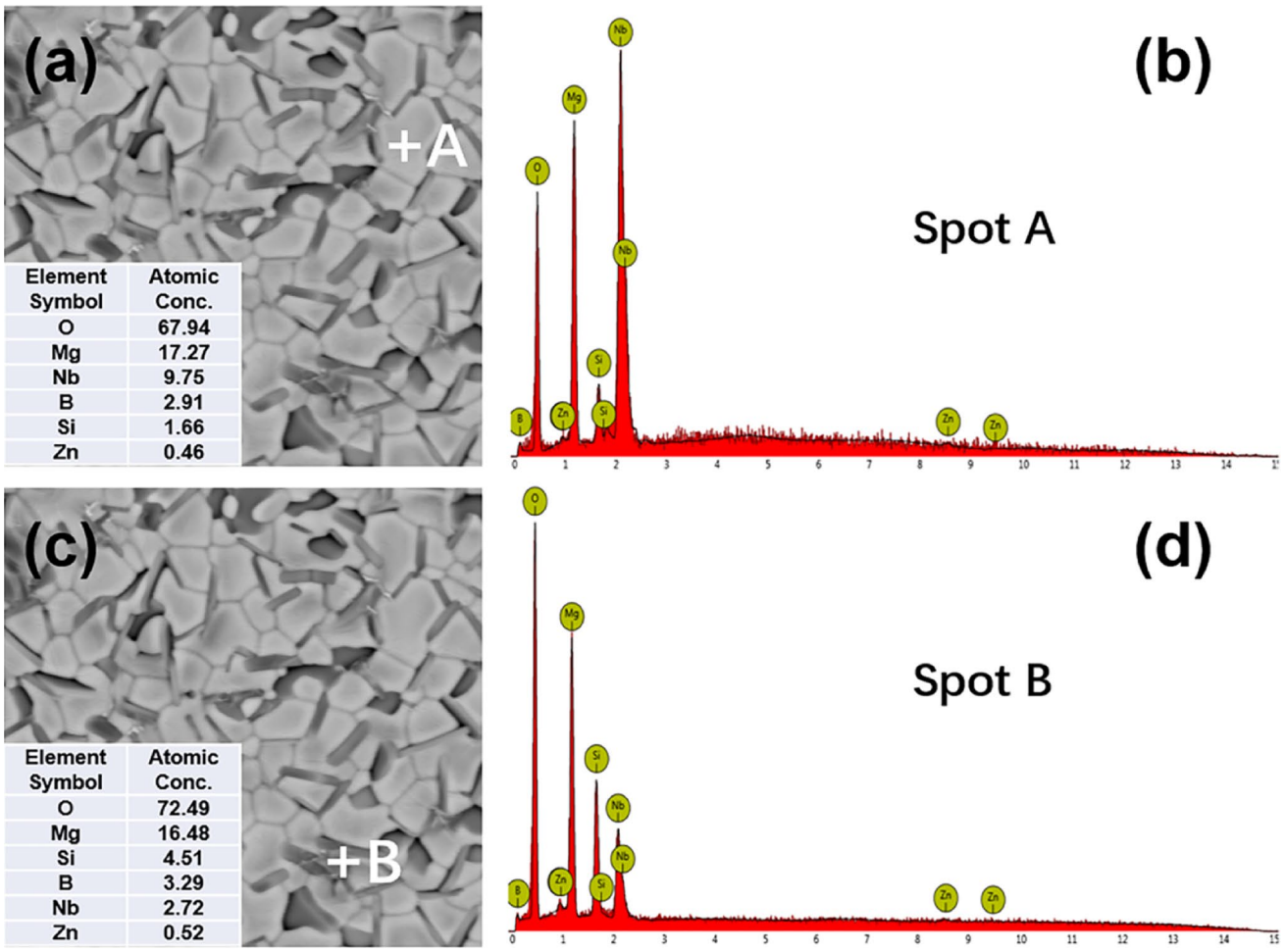

Fig. 4 The EDS analysis of $Li_3Mg_2NbO_6$ ceramics doped with 4 wt% LMZBS glass sintered at 925 °C for 4 h. **a**, **b** EDS analysis on A spot, and **c**, **d** EDS analysis on B spot

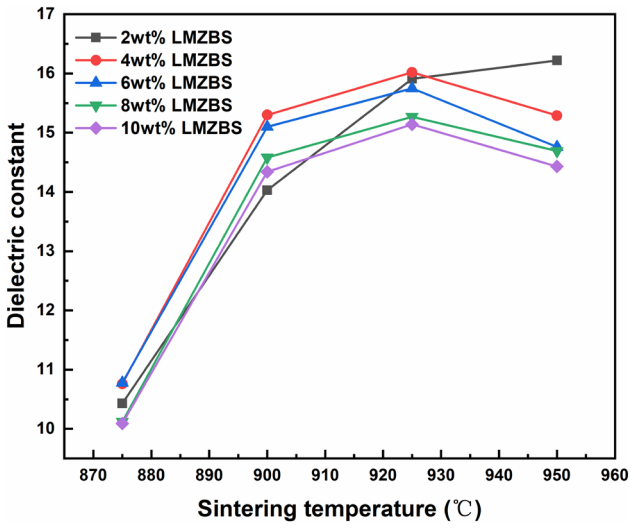

Fig. 5 The Dielectric constants of the $Li_3Mg_2NbO_6+x$ wt% LMZBS ($x=2$–10) ceramics sintered at 875–950 °C for 4 h

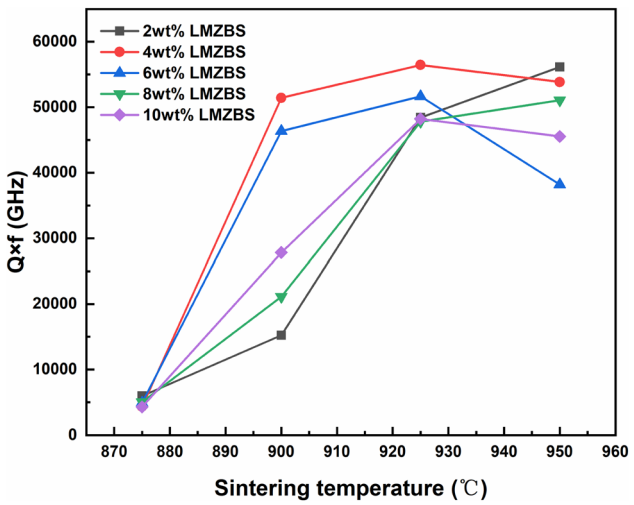

Fig. 6 The $Q\times f$ values of the $Li_3Mg_2NbO_6+x$ wt% LMZBS ($x=2$–10) ceramics sintered at 875–950 °C for 4 h

doping 4 wt% LMZBS glass sintering at 925 °C for 4 h. In general, the $Q \times f$ value is affected by inherent loss and external loss [22]. The inherent loss is mainly related to the structure and the type of the crystals. The external loss is related to the densification, secondary phase, grain size, and porosity [23]. Therefore, the change of quality factor can be attributed to the sintering temperature and the doping of the LMZBS glass, and both of them leading to changes in the ceramic density, the appearance of impure phases and the changes in grain size.

The temperature coefficient of frequency is not sensitive to the sintering temperature, but it is related to the phase composition of ceramics themselves, additives, and other phases [24]. Figure 7 displays the temperature coefficient of resonance frequency changes with the content of LMZBS glass. The results display that with the increase of LMZBS glass content, the value of τ_f shifts toward the negative direction. Therefore, the reason for the decrease in the value of τ_f may be due to the addition of LMZBS glass leading to the appearance of impure phases. Besides, the temperature coefficient of frequency of the LMZBS glass materials is a negative value [25].

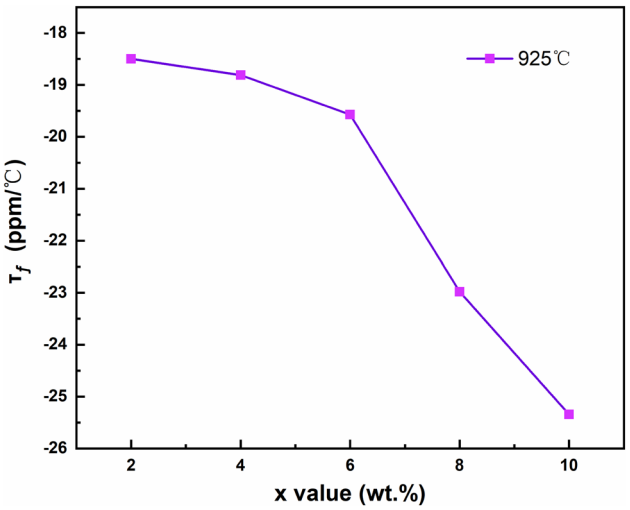

Fig. 7 The τ_f value of the $Li_3Mg_2NbO_6 + x$ wt% LMZBS ($x = 2$–10) ceramics sintered at 925 °C for 4 h

The comparison of microwave dielectric properties of some typical the low sintering of $Li_3Mg_2NbO_6$-based systems is illustrated in Table 2 ($Li_3Mg_2NbO_6 + 0.1$ wt% B_2O_3 [26], $Li_3Mg_2NbO_6 + 0.5$ wt%ZBS [27], $Li_3Mg_2NbO_6 + 0.1$ wt%$BaCu(B_2O_5)$ [28], $0.7Li_3(Mg_{0.92}Zn_{0.08})_2NbO_6 + 0.3Ba_3(VO_4)_2$ [29], $Li_3Mg_2NbO_6$ by the HEBM method [30]). It is observed that $Li_3Mg_2NbO_6 + 4$ wt% LMZBS ceramics have low sintering temperatures and high $Q \times f$ value. Figure 8 shows the cross-section SEM photograph and the EDS face scan of $Li_3Mg_2NbO_6 + 4$ wt% LMZBS glass co-fired with silver electrode at 925 °C for 4 h. It can be seen from Fig. 8a that there is a clear boundary between the silver electrode and the composite ceramics, which indicates that there is no obvious chemical reaction between the composite ceramics and the silver electrode. The results of EDS face scan from Fig. 8b show that there was no diffusion of silver electrode during the co-firing process. Therefore, $Li_3Mg_2NbO_6 + 4$ wt% LMZBS ceramics have excellent microwave dielectric properties and compatibility with silver electrode. The composite ceramics are suitable materials for LTCC applications.

4 Conclusion

In summary, $Li_3Mg_2NbO_6 + x$ wt% Li_2O–MgO–ZnO–B_2O_3–SiO_2 (LMZBS, $x = 2$–10) composite ceramics were synthesized at 875–950 °C by traditional the solid-state method, and the effects of LMZBS glass on the sintering temperature, phase composition, and dielectric properties of $Li_3Mg_2NbO_6$ ceramics were studied in this work. From the research results, it was proved that the $Li_3Mg_2NbO_6$ ceramics doped with the Li_2O–MgO–ZnO–B_2O_3–SiO_2 glass could effectively reduce the sintering temperatures of the ceramics and increase the density of the materials. The prepared materials also had excellent dielectric properties, in particular, $Li_3Mg_2NbO_6 + 4$ wt% LMZBS ceramics exhibited excellent microwave dielectric properties when sintered at 925 °C for 4 h of $\varepsilon_r = 16.02$, $Q \times f = 56{,}455$ GHz (8.361 GHz), $\tau_f = -18.81$ ppm/°C. The composite ceramics show compatibility with Ag electrode and meet the requirements of LTCC applications.

Table 2 The comparison of microwave dielectric properties of some typical the low sintering of $Li_3Mg_2NbO_6$-based systems

Material systems	*S. T* (°C)	ε_r	$Q \times f$ (*GHz*)	τ_f (*ppm/°C*)
$Li_3Mg_2NbO_6 + 0.1$ wt% B_2O_3	925	14.0	67,451	− 16.82
$Li_3Mg_2NbO_6 + 0.5$ wt% ZBS	925	14.84	73,987	− 16.05
$Li_3Mg_2NbO_6 + 0.1$ wt% $BaCu(B_2O_5)$	950	14.27	55,521	− 18.2
$0.7Li_3(Mg_{0.92}Zn_{0.08})_2NbO_6 + 0.3Ba_3(VO_4)_2$	950	16.3	50,084	+ 1.5
$Li_3Mg_2NbO_6$ by the HEBM method	950	18.0	51,870	− 23.01
This work	925	16.02	56,455	− 18.81

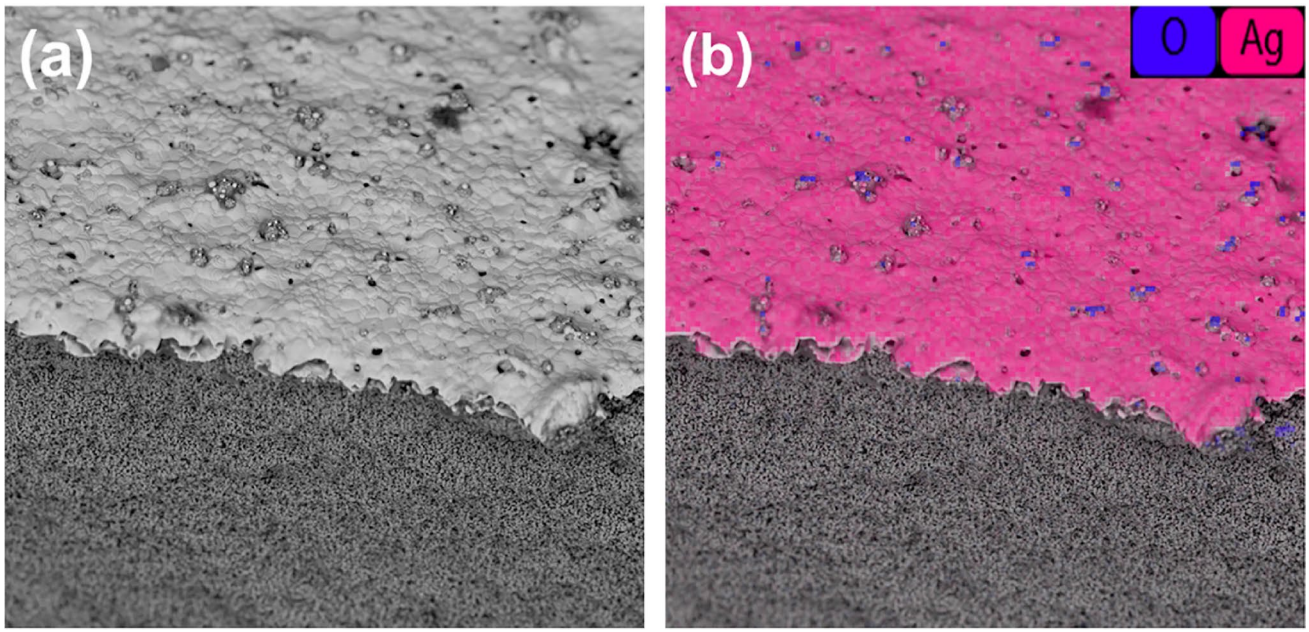

Fig. 8 The cross-section SEM photograph (**a**) and the EDS face scan (**b**) of $Li_3Mg_2NbO_6$ + 4 wt% LMZBS glass co-fired with silver electrode at 925 °C for 4 h

References

1. I.M. Reaney, D. Iddles, J. Am. Ceram. Soc. **89**, 2063–2072 (2006)
2. E.T. Thostenson, T.W. Chou, Compos. Pt. A-Appl. Sci. Manuf. **30**, 1055–1071 (1999)
3. M.T. Sebastian, H. Jantunen, Int. Mater. Rev. **53**, 57–90 (2008)
4. Y.P. Pu, J.W. Li, X.Y. Wang, Y. Shi, R.K. Shi, M.D. Yang, W. Wang, X. Guo, X. Peng, Compos. Sci. Technol. **186**, 9 (2020)
5. L. Zhang, Y.P. Pu, M. Chen, Ceram. Int. **46**, 98–105 (2020)
6. R.K. Shi, Y.P. Pu, W. Wang, X. Guo, J.W. Li, M.D. Yang, S.Y. Zhou, J. Alloy. Compd. **815**, 8 (2020)
7. H.S. Ren, L. Hao, H.Y. Peng, M.Z. Dang, T.Y. Xie, Y. Zhang, S.H. Jiang, X.G. Yao, H.X. Lin, L. Luo, J. Eur. Ceram. Soc. **38**, 3498–3504 (2018)
8. H.S. Ren, S.H. Jiang, M.Z. Dang, T.Y. Xie, H. Tang, H.Y. Peng, H.X. Lin, L. Luo, J. Alloy. Compd. **740**, 1188–1196 (2018)
9. G. Wang, D.N. Zhang, X. Huang, Y.H. Rao, Y. Yang, G.W. Gan, Y.M. Lai, F. Xu, J. Li, Y.L. Liao, C. Liu, L.C. Jin, V.G. Harris, H.W. Zhang, J. Am. Ceram. Soc. **103**, 214–223 (2020)
10. P. Zhang, K.X. Sun, M. Xiao, Z.T. Zheng, J. Am. Ceram. Soc. **102**, 4127–4135 (2019)
11. L.L. Yuan, J.J. Bian, Ferroelectrics **387**, 123–129 (2009)
12. H.L. Pan, Y.X. Mao, L. Cheng, H.T. Wu, J. Alloy. Compd. **723**, 667–674 (2017)
13. P. Zhang, H. Xie, Y.G. Zhao, X.Y. Zhao, M. Xiao, J. Alloy. Compd. **690**, 688–691 (2017)
14. G. Wang, H.W. Zhang, C. Liu, H. Su, L.J. Jia, J. Li, X. Huang, G.W. Gan, J. Electron. Mater. **47**, 4672–4677 (2018)
15. G. Wang, H.W. Zhang, C. Liu, H. Su, J. Li, X. Huang, G.W. Gan, F. Xu, Mater. Lett. **217**, 48–51 (2018)
16. T.Y. Qin, C.W. Zhong, H.C. Yang, Y. Qin, S.R. Zhang, Ceram. Int. **45**, 10899–10906 (2019)
17. M.X. Wang, C.W. Zhong, T.Y. Qin, Q. Yang, B. Tang, S.R. Zhang, Ceram. Int. **46**, 12088–12095 (2020)
18. P.L. Wang, M. Zhu, Y. Chen, F. Xie, N. Xiao, B. Hou, W. Lu, F.W. Jiang, W.Z. Zheng, Mater. Res. Express **6**, 8 (2019)
19. Y.V. Bykov, K.I. Rybakov, V.E. Semenov, J. Phys. D-Appl. Phys. **34**, R55–R75 (2001)
20. S. George, M.T. Sebastian, J. Alloy. Compd. **473**, 336–340 (2009)
21. Y.C. Liou, Y.C. Wu, J. Electron. Mater. **46**, 2387–2392 (2017)
22. X.H. Zhou, L.X. Xue, H.B. Sun, H.Y. Yang, S.R. Zhang, J. Mater. Sci.-Mater. Electron. **29**, 643–649 (2018)
23. H.B. Bafrooei, M. Feizpour, A. Sayyadi-Shahraki, K.X. Song, J. Alloy. Compd. **834**, 9 (2020)
24. L.X. Li, Z.D. Gao, Y.R. Liu, H.C. Cai, S. Li, Mater. Lett. **140**, 5–8 (2015)
25. L.S. Xie, C.W. Zhong, Z.X. Fang, Y. Zhao, B. Tang, S.R. Zhang, J. Ceram. Soc. Jpn. **126**, 163–169 (2018)
26. P. Zhang, J.W. Liao, Y.G. Zhao, X.Y. Zhao, M. Xiao, J. Mater. Sci.-Mater. Electron. **28**, 686–690 (2017)
27. P. Zhang, L. Liu, Y.G. Zhao, M. Xiao, J. Mater. Sci.-Mater. Electron. **28**, 5802–5806 (2017)
28. C. Luo, Y.D. Hu, S.X. Bao, T. Hong, L.B. Ai, J. Chen, Z.Z. Duan, J. Mater. Sci.-Mater. Electron. **29**, 15523–15528 (2018)
29. T.W. Zhang, R.Z. Zuo, C. Zhang, Mater. Res. Bull. **68**, 109–114 (2015)
30. L.P. Zhao, P. Liu, G.Q. Sun, Z.F. Fu, J. Mater. Sci.-Mater. Electron. **29**, 5873–5877 (2018)